# Comparative analysis of three generations of LYSO:Ce crystals for medical imaging applications

Wehr, Jack; van Blaaderen, J. Jasper; Rasch, Coen R.N.; Schaart, Dennis R.

**DOI**
10.1016/j.nima.2025.170919

**Publication date**
2026

**Document Version**
Final published version

**Published in**
Nuclear Instruments and Methods in Physics Research, Section A: Accelerators, Spectrometers, Detectors and Associated Equipment

**Citation (APA)**
Wehr, J., van Blaaderen, J. J., Rasch, C. R. N., & Schaart, D. R. (2026). Comparative analysis of three generations of LYSO:Ce crystals for medical imaging applications. *Nuclear Instruments and Methods in Physics Research, Section A: Accelerators, Spectrometers, Detectors and Associated Equipment*, *1082*, Article 170919. https://doi.org/10.1016/j.nima.2025.170919

Nuclear Instruments and Methods in Physics Research A 1082 (2026) 170919

Contents lists available at ScienceDirect

Nuclear Inst. and Methods in Physics Research, A

journal homepage: www.elsevier.com/locate/nima

Full Length Article

# Comparative analysis of three generations of LYSO:Ce crystals for medical imaging applications

Jack Wehr [a,*], J. Jasper van Blaaderen [a], Coen R.N. Rasch [b,c], Dennis R. Schaart [a,c]

[a] Delft University of Technology, 2629JB, Delft, The Netherlands
[b] Leiden University Medical Centre, 2333ZA, Leiden, The Netherlands
[c] HollandPTC, 2629JH, Delft, The Netherlands

ARTICLE INFO

*Keywords:*
LYSO:Ce
Scintillation crystals
PET detectors
Time-of-flight PET
Digital SiPM
Cramér-Rao lower bound

ABSTRACT

The refinement of high-performing scintillator compounds is critical to the advancement of time-of-flight positron emission tomography (TOF-PET). Here, we characterize 2nd, 4th, and 5th generation cerium-doped, calcium co-doped lutetium–yttrium oxyorthosilicate (LYSO) crystals developed and supplied by Luxium Solutions in terms of light yield, emission spectra, non-proportionality, and decay time. Additionally, the samples are coupled to a Philips 3200 digital photon counter (DPC) for a comparison of performance as a detector component. The detector sensitivity, energy resolution, and coincidence resolving time (CRT) of the crystals are measured at −25 °C. The 4th and 5th generation crystals are shown to have similar light yields and decay times at room temperature, and outperform the 2nd generation crystals in all measured characteristics. The detectors making use of 5th generation crystals had markedly better sensitivity, energy resolution, and CRT values than their 4th generation counterparts.

## 1. Introduction

Scintillation crystals with superior properties are key to improving image quality in positron emission tomography (PET) detectors [1]. A high light-yield, together with short rise and decay times, allow for accurate determination of the time of interaction, leading to high-precision time-of-flight PET (TOF-PET). The timing performance can be directly measured as the coincidence resolving time (CRT) of a system. A high light-yield is furthermore crucial to accurate event positioning, while good energy resolution is important for pulse analysis and event discrimination.

One envisioned application for PET technology is the enhancement of proton therapy for cancer treatment, which has thus far been hampered by the lack of methodologies for validation of beam range during treatment. Proton therapy is seen as a promising technology in radiation therapy due to its localized deposition of energy, which has the potential to better spare healthy tissue around the tumor. Unfortunately, this also has the consequence of delivering increased dose outside the target area if the beam is off-target compared with photon-based treatment. Additionally, it is more difficult to verify beam positioning because traditional methods of verification which rely on the exit dose cannot be used. Since one of the products of the interaction of the proton beam with tissue is the generation of positrons, PET technology could be employed as a technique for range verification during treatment [2–8]. It has been shown on the basis of Monte Carlo simulations that a dual-panel PET detector with a timing resolution on the order of 200 ps would be compatible with clinical particle therapy solutions while providing artifact-free images [9,10]. This work describes the selection and characterization of a scintillator material for use in such a detector.

We determine and compare the characteristics of the 2nd, 4th, and 5th generations of cerium and calcium-doped lutetium–yttrium oxyorthosilicate $(Lu_{0.9}Y_{0.1})_2SiO_5:Ce^{3+}$, $Ca^{2+}$ (LYSO) crystals developed and supplied by Luxium Solutions. The generation 2, 4, and 5 crystals have $Ce^{3+}$ concentrations of 0.022%, 0.003%, and 0.25% respectively. The crystals contain proprietary concentrations of $Ca^{2+}$. The generation 2 crystals have a very low $Ca^{2+}$ concentration and their scintillation properties are therefore expected to be close to those of classical, non-codoped LYSO:Ce. Generations 4 and 5 have a higher $Ca^{2+}$ concentration, such that a higher light yield and faster decay are expected [11]. Generation 5 has the highest $Ca^{2+}$ concentration of the three generations. The crystals are etched on all faces except one. The performance of these materials as scintillators in a PET detector is investigated in a small-scale setup using a Philips digital silicon photomultiplier model

* Corresponding author.
*E-mail addresses:* j.wehr@tudelft.nl (J. Wehr), j.j.vanblaaderen@tudelft.nl (J.J. van Blaaderen), c.r.n.rasch@lumc.nl (C.R.N. Rasch), d.r.schaart@tudelft.nl (D.R. Schaart).

https://doi.org/10.1016/j.nima.2025.170919
Received 12 May 2025; Received in revised form 24 July 2025; Accepted 30 July 2025
Available online 7 August 2025

DPC-3200-22, which has been extensively used in the past for similar measurements, e.g. van Dam et al. [12] and Borghi et al. [13].

## 2. Methods

### 2.1. Crystal characteristics

Experiments were performed on crystals of two sizes: 3.3 mm × 3.3 mm × 5 mm and 3.3 mm × 3.3 mm × 3.3 mm. The smaller crystals were used to measure light yield, emission spectrum, and decay time. The larger crystals were used in CRT measurements, energy resolution measurements, and temperature-dependent light yield measurements performed on the digital photon counter (DPC). A low-activity background due to the $^{176}$Lu content of the crystals was assumed, and considered negligible.

Pulse height spectra for each of the samples were measured at room temperature using a Hamamatsu R1791 photomultiplier tube (PMT). The crystal to be measured was placed on the window of the PMT without optical coupling, and a covering of Teflon tape was arranged to cover the sample and entire window. A 0.9 MBq $^{22}$Na source was then placed directly on the Teflon covering. A value for the number of photoelectrons per scintillation event was calculated from the channel number corresponding to the photopeak and the single electron response of the PMT. A value for the light yield was obtained by taking into account the reflectivity and quantum efficiency of the PMT. A more detailed account of the apparatus and methodology is presented by de Haas et al. [14].

Pulsed X-ray excited decay time measurements were performed at room temperature using a time-correlated single-photon counting method described in [15]. In brief, a start signal was recorded with the triggering of a PicoQuant LDH–P-C440 M laser diode. This excited a Hamamatsu N5084 X-ray tube, which emitted a pulse of X-rays incident on the sample at a distance of 5 cm. An ID Quantique ID100–50 single-photon detector was used to detect the scintillation photons and generate a stop signal. The processing of start and stop signals was performed by an Ortec 567 time-to-amplitude converter, and the output digitized by an Ortec AD 144 16K ADC. The differences between the timestamps of the corresponding start and stop signals were plotted, and a decay curve was formed. Fitting the decay curve with an exponential model allowed for a determination of the decay time. It was ensured that there was at least a factor of $10^5$ more start signals than stop signals, so that on average for each event only one scintillation photon would be detected. Were this not the case a bias would be introduced into the data, since if multiple photons were incident on the photodetector, only the stop signal of the first would be recorded.

X-ray excited emission spectra were recorded using an X-ray tube with a tungsten anode operated at 79 kV, producing an average X-ray energy of 40 keV at a distance of 3 cm from the samples. A 3 mm aluminum filter was used to remove low energy X-rays to prevent damage to the samples. The resulting scintillation photons were coupled into an optical fiber, and analyzed by an Ocean Optics QE65-pro spectrometer. Further description of this setup can be found in van Blaaderen et al. [16] and van Aarle et al. [17].

### 2.2. Scintillation detector measurements

The photosensor was a model DPC-3200-22-44 digital SiPM developed by Philips Digital Photon Counting (PDPC). Fig. 1 shows an overview of the instrumentation layout. Detailed information regarding the dSiPM is available elsewhere and will not be discussed in depth here [18–20]. It consists of 16 dies in a 4 × 4 configuration, each of which is capable of semi-independent operation. Each die is composed of four 3.2 mm × 3.8755 mm pixels, as well as a time-to-digital converter (TDC). Each of the pixels contains 3200 single-photon avalanche diodes (SPADs), which can be individually read out. It is also possible to selectively disable a specified percentage of SPADs which have the highest dark count rates. A die is therefore capable of recording one timestamp and four values corresponding to the number of SPADs activated in each pixel. Each of the four pixels in a die contains four sub-pixels, which can be used to set trigger conditions. These sub-pixels are in turn composed of groups of row-trigger-lines, which can be grouped and used to set validation conditions.

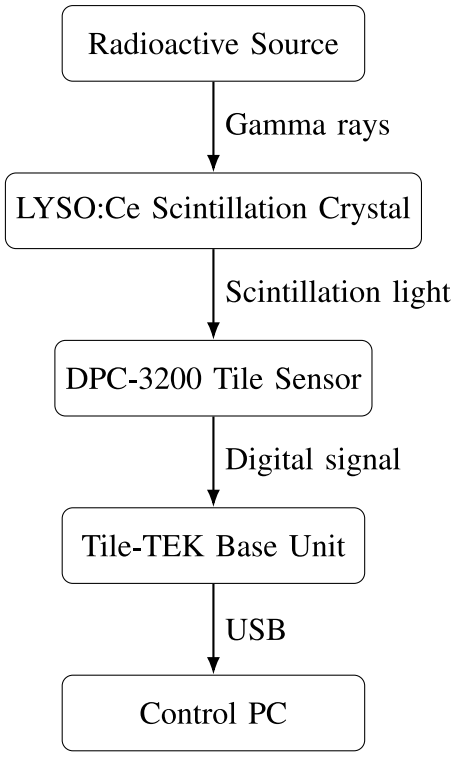


**Fig. 1.** Block diagram of the DPC-3200 readout system.

The event acquisition sequence begins once the trigger conditions are met. This occurs when a certain number of SPADs are activated in each sub-pixel, or when photons are detected in a specific combination of sub-pixels, depending on the trigger logic set. The TDC records a timestamp when an event is triggered. The trigger must be validated within a configurable time-window for the event to be recorded. The validation conditions are met when a specific combination of row-trigger-line groups defined by a trigger scheme are activated. If the event is validated, the detector waits for a specified time to allow photons from the event to accumulate. Finally, the signal is read out and the sensor is recharged. A coincidence window can also be implemented to remove events which do not have any corresponding events within the specified window.

For the experiments described in this work, the following settings were used: the DPC was set to first photon triggering, the validation requirement was set to scheme 4, the integration time was set to 165 ns, and the coincidence time window was set to 4 ns. The over-voltage was set to 2 V. The noisiest 5% of SPADs were deactivated. These settings mimic those of van Dam et al. [12], who measured the CRT of small $Ca^{2+}$-codoped LSO:Ce crystals in a similar setup.

The measurements were conducted in a light-tight, temperature controlled chamber. The temperature was stabilized to −25 °C ± 0.5 °C using a Peltier element. Eljen EJ-550 silicone grease was used to optically couple the polished faces of the crystals to the tile, and teflon tape was wrapped around the crystals to increase the number of scintillation photons incident on the sensor.

Due to the mismatch between the crystal and pixel faces - 3.3 mm × 3.3 mm and 3.2 mm × 3.8755 mm, respectively - a fraction of the scintillation photons would be lost with a one-to-one crystal to pixel

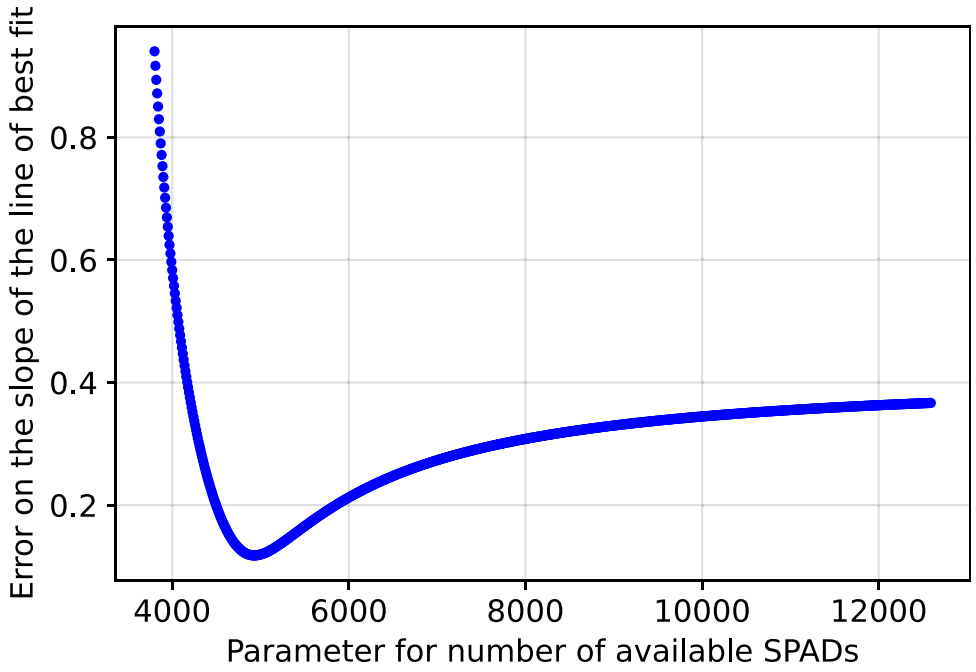


**Fig. 2.** Curve for the determination of the number of SPADs available to detect light from the coupled crystal. The line of best fit through the saturation-corrected calibration curve had its error minimized with a value of available SPADs of about 4900.

coupling. A coupling of one crystal to two pixels - 6.4 mm × 3.8755 mm - was investigated, however this too was found to lose a considerable number of photons to neighboring deactivated pixels. The best timing performance was achieved by coupling crystals to the center of dies, one-to-one. The large number of photons detected with respect to the other two methods more than compensated for the additional electronic jitter associated with activating all four pixels in the die. This is a key difference from van Dam et al. [12], whose 3 mm × 3 mm LYSO crystals would likely have a more favorable light distribution over a single activated pixel.

Saturation effects were dealt with using the method described by van Dam et al. [21]. The crosstalk probability was taken to be 0.18, and the dark counts were assumed to be negligible since the measurements were performed at −25 °C [12]. A value for the total number of available SPADs which scintillation photons can activate is required for the correction. To this end, low-activity sources at various energies from 31 keV to 662 keV were used to generate calibration curves. The number of SPADs activated at the center of the photopeaks of the pulse height spectrum of these sources were measured. Data for higher-energy sources was also taken, however the saturation effects became so pronounced that the photopeak could not be resolved with a Gaussian fit. The value for the available number of SPADs was then determined by choosing a number which minimized the error of a straight-line fit to the saturation-corrected data (Fig. 2). This method was used for each generation of LYSO crystals, since their unique light yields resulted in inherently different calibration curves.

Energy resolutions were measured twelve at a time by arranging the crystals as shown in Fig. 3. A 0.9 MBq $^{22}$Na source was placed in the centre of the detector. Four crystals from each generation were measured at varying distances of approximately 14–17 mm from the source, and energy spectra were recorded. A calibration curve was generated using sources which had emissions between 31 keV and 662 keV. After correction for saturation, values of the slope and intercept for the calibration curve were used to convert values for numbers of SPADs activated to keV (Fig. 4). The energy resolution of the crystals was then obtained by taking the FWHM of the Gaussian fit to the photopeak of the measurement after energy calibration, and using the equation:

$$E_{Res} = \frac{\Delta E}{E} \quad (1)$$

No significant scattering from neighboring crystals was detected in this configuration, and scattered events were expected to occur outside the photopeak.

The temperature-dependent light yield was measured using the same configuration. A Peltier element was used to achieve an accurate and constant temperature over the detector tile for the duration of each measurement. Light yield measurements were taken between −30 °C and 25 °C. It should be noted that the dark count map was measured at −25 °C and was not updated at each temperature interval. It is possible that some SPADs that had low dark count rates at −25 °C may have had disproportionately larger dark count rates at higher temperatures, and that the inhibit map did not accurately disable the noisiest 5% of SPADs. This effect is expected to be of minimal importance to the results.

Owing to the differing timing performance between different pairs of dies, it was not possible to take advantage of the crystal arrangement depicted in Fig. 3 to measure the coincidence resolving time. Instead, crystal pairs were measured one at a time, using the same pair of dies. The setup was otherwise the same, with the exception that the source was placed directly between the crystals, at a distance of 12 mm, so that coincident events could be detected. Only events that were located within the full-width-at-tenth-maximum (FWTM) of the obtained full-energy peak were accepted. A coincidence filter was applied to the data offline.

Timestamp differences between detected photons in each event were plotted, and the resulting histogram was fit with a Gaussian curve (Fig. 5). The full-width-at-half-maximum (FWHM) of this fit was obtained, which is defined as the CRT of the detector.

## 3. Results and discussion

### 3.1. Crystal characteristics

The light yield of eight crystals of each generation were measured with a PMT as described in 2.1 (Fig. 6). The averages of the results for generations 2, 4, and 5 are shown in Table 1. The generation 4 and 5 crystals showed a higher light yield than the generation 2 crystals.

Fig. 7 shows the emission spectra of the three generations of crystals. It can be seen that generation 4 crystals peak at around 425 nm

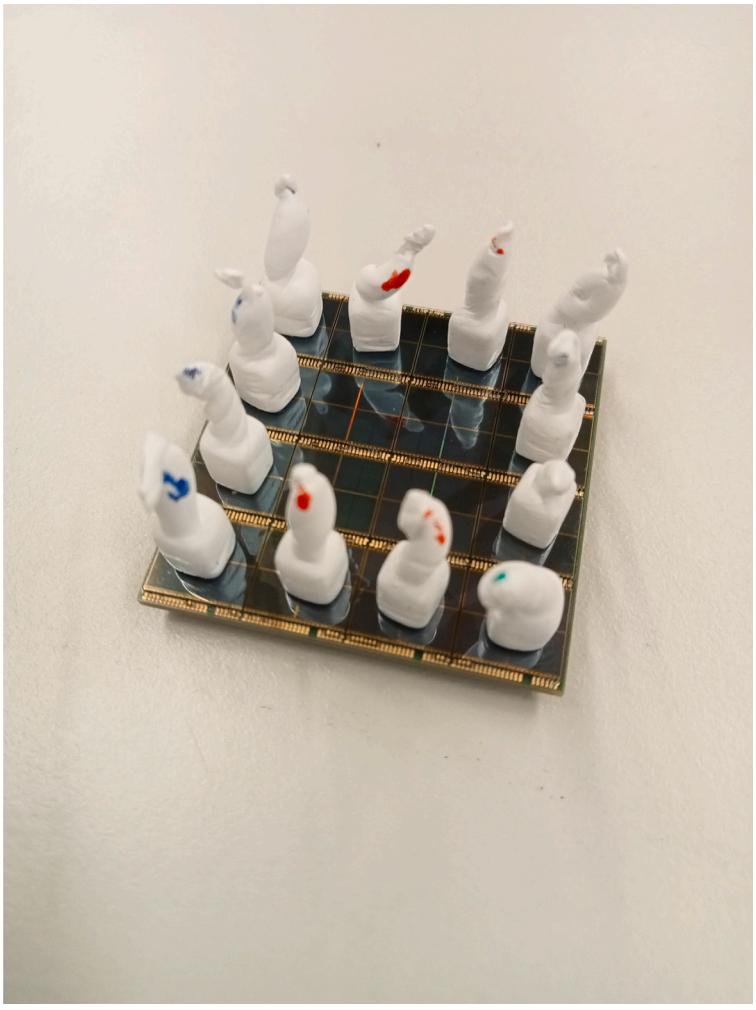

**Fig. 3.** Image of a DPC tile with twelve crystals positioned over the centers of dies. During measurements, a source would be placed in the center of the configuration.

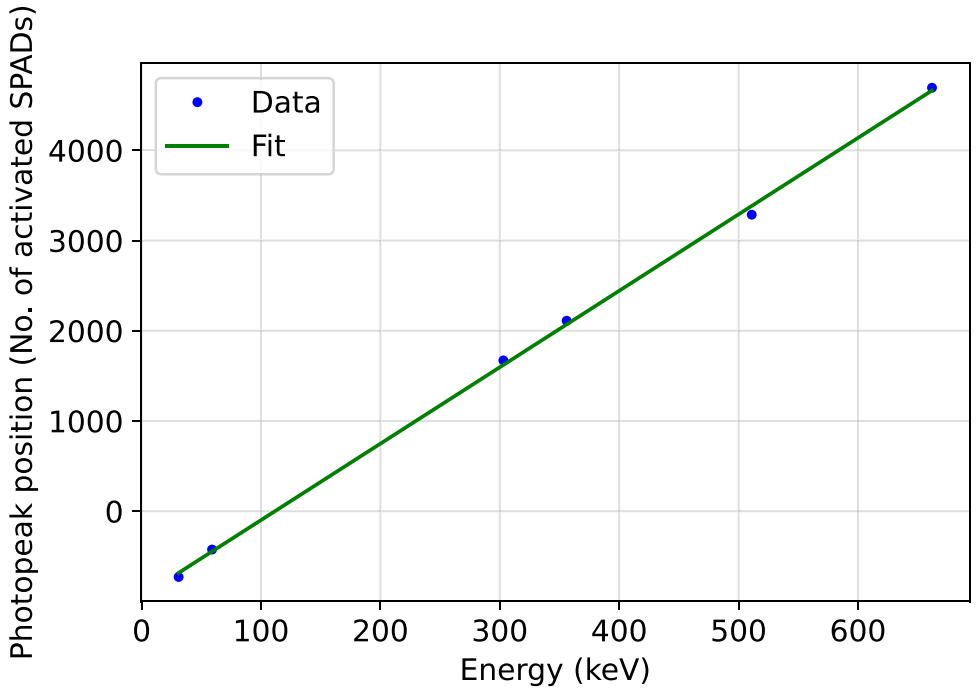


**Fig. 4.** Calibration curve for a detector using a generation 5 crystal.

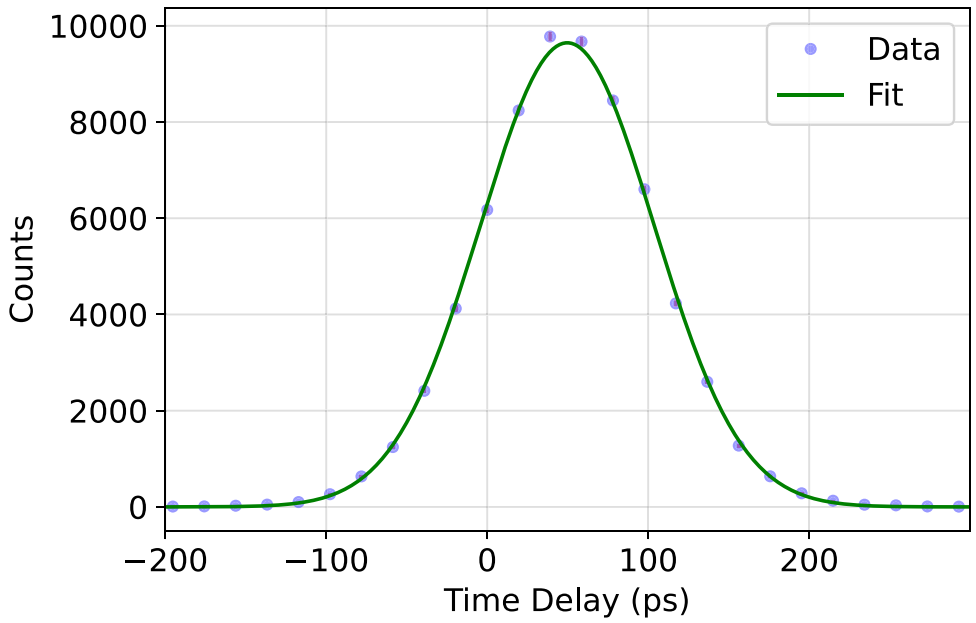


**Fig. 5.** Coincidence timing spectrum of two generation 5 crystals fit with a Gaussian curve.

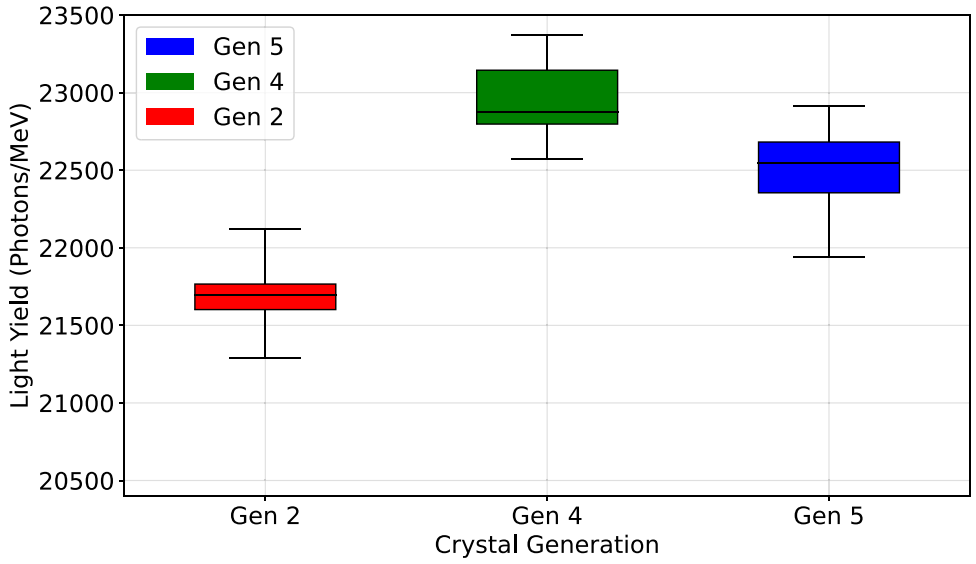


**Fig. 6.** Light yield measurements for the three generations of LYSO crystals at room temperature using a PMT.

- slightly shorter than the peak wavelength than the generation 2 and 5 crystals. The Philips DPC has a sharp drop-off in PDE around this region [22].

The non-proportional response of the materials shown in Fig. 8 was measured using $^{137}$Cs, $^{22}$Na, $^{133}$Ba, $^{60}$Co, and $^{241}$Am sources. The horizontal line indicates uniform proportionality. It can be seen that the response is relatively uniform between 500 keV and 1 MeV but sublinear at lower energies. A dip can be seen at 81 keV, which is likely due to altered ionization cascades near the lutetium K-edge (63.3 keV). This reduces scintillation efficiency due to changes in energy deposition mechanisms. These results are consistent with previous work in the field [23–25]. The generation 5 crystals showed improved non-proportionality over the other two generations.

Fig. 9 shows decay time measurements for eight crystals from each generation. The average values for generations 2, 4, and 5 are shown in Table 1. The generation 4 and 5 crystals performed similarly, with a noticeably faster decay than the generation 2 crystals. Given the degree of uncertainty and the range of values for each crystal in the generations, it is not possible to make a statement regarding whether generation 4 or generation 5 has a faster decay time.

### 3.2. Scintillator detector results

A temperature-dependent measurement was also carried out on the DPC, which showed no significant change in light yield between −25 °C and 30 °C for any of the generations. It can be seen in Fig. 10 that the light yields of the various generations rise and fall together at each temperature point. These slight variations of the observed light yield are attributed to the adjusting of the bias voltage of the DPC between measurements at different temperatures.

It can be seen from Fig. 10 that the generation 5 crystals appear to emit more light than their generation 4 counterparts, contrary to the results of the experiments conducted using the PMT (Fig. 6). This is partially attributed to the better matching of the scintillation photon emission spectrum to the photodetection efficiency (PDE) curve of the DPC in generation 5, which can be seen in Fig. 7. Another contributing

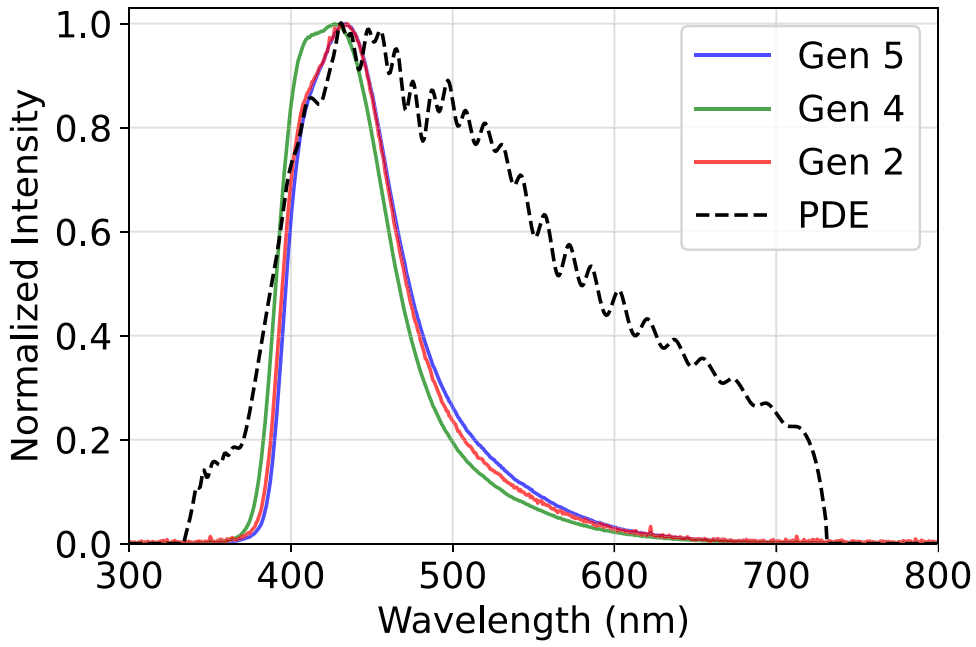


**Fig. 7.** Emission spectra for the different generations of crystals. The normalized PDE of the DPC is displayed alongside the spectra for comparison. *Source:* PDE data adapted from [22].

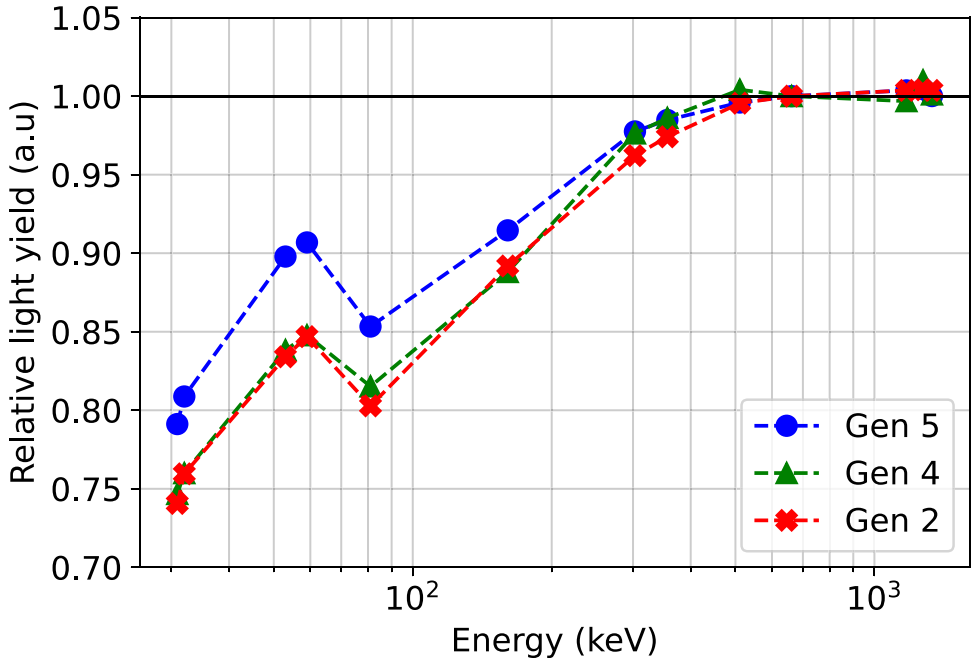


**Fig. 8.** Non-proportionality curves for the various generations of LYSO crystals, measured using a PMT at room temperature. $^{137}$Cs, $^{22}$Na, $^{133}$Ba, $^{60}$Co, and $^{241}$Am sources were used. The solid line at 1 marks the reference level corresponding to normalization at 662 keV. The dip observed at 81 keV is attributed to changes in electron cascade processes near the lutetium K-edge at 63.3 keV, which affect ionization density and scintillation efficiency.

factor could be the difference in Teflon wrapping between the two experimental setups. The crystals were tightly wrapped when coupled to the DPC, however when measured by the PMT they were covered along with the surface of the PMT. A larger fraction of scintillation photons may therefore have been absorbed by any impurities on the Teflon or surfaces of the crystals while coupled to the DPC, which would have a disproportionately larger impact on the shorter wavelength of the generation 4 emission spectrum.

The energy resolution of four crystals of each type was measured in a range of energies between 31 keV and 662 keV by arranging the setup depicted in Fig. 3 and placing a source in the center of the tile. Example spectra can be seen in Fig. 11, and the average of each generation across the energy range is shown in Fig. 12. The purpose of this study is directed toward PET applications, and therefore the energy resolution at 511 keV is of particular interest. The energy resolutions measured at 511 keV for generations 2, 4, and 5 are given in Table 2. Since the energy resolution is dominated by the light yield, the trends and relative differences between the generations were expected, given the light yield measurements conducted on the DPC and the non-proportionality measurements conducted on the PMT previously. As anticipated, the energy resolutions of the crystals are proportional to the inverse of the square root of the light yield; however, the fifth-generation crystals

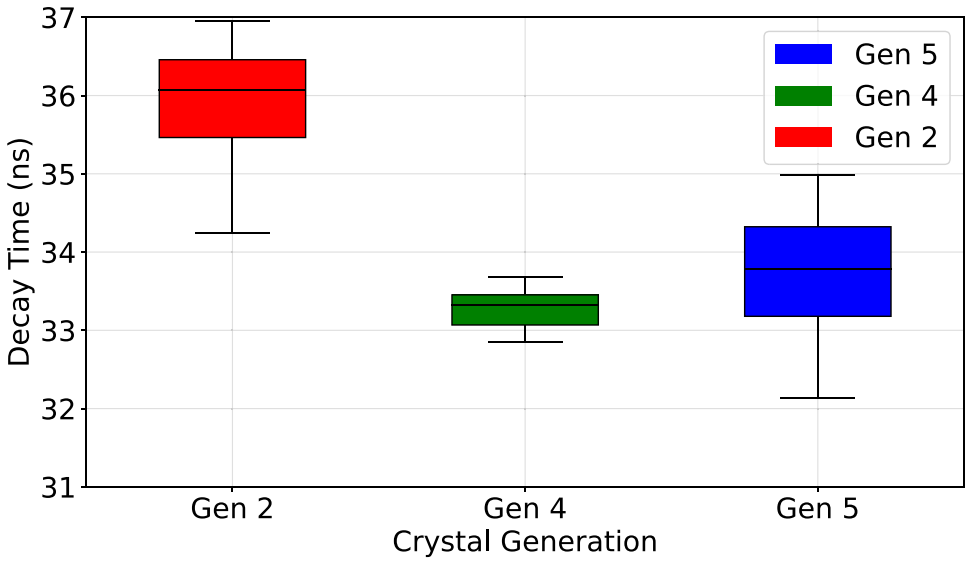


**Fig. 9.** Decay times for crystal samples of the three generations at room temperature.

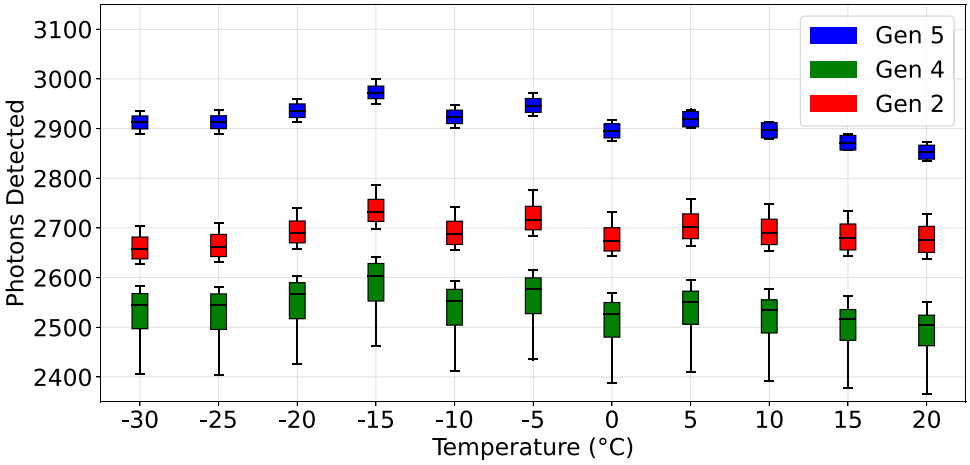


**Fig. 10.** Temperature-dependent light yield measurements for the three generations of LYSO crystals mounted on a DPC. Each point represents the average value for four crystals.

exhibit improved energy resolution beyond this trend, which can be attributed to their superior non-proportionality [26].

CRT measurements can be seen in Fig. 13. The best value of CRT obtained was 126.3 ± 0.7 ps FWHM from a generation 5 crystal. For reference, van Dam et al. [12] obtained values between 120 ps and 131 ps FWHM using pairs of LSO:Ce,0.2%Ca crystals and a similar but distinct setup using the same DPC model. Additional measurements were carried out on the same samples described in that paper, using the crystal-to-die coupling used for the other crystals in this work, and values of 136.4 ps, 129.6 ps, and 123.2 ps FWHM were obtained. The measurements were repeated with the same crystals and crystal-pixel coupling used by van Dam et al. and were measured to be 147.6 ps, 135.9 ps, and 129.2 ps FWHM respectively. It is thought that the discrepancy between the latter values and the ones reported by van Dam et al. [12] is due to degradation of the optical quality of the sample surfaces, which was visually apparent.

### 3.3. Cramer–Rao lower bound analysis

Cramer–Rao lower bound (CRLB) analysis was carried out to determine the contributions of the various properties of the crystals to the CRT obtained with the crystal-detector combination. Custom Python code was developed for these calculations and is available at https://doi.org/10.6084/m9.figshare.28945925 [27]. The CRLB on the time of interaction $\Theta$ equals the minimum value of the variance that any unbiased estimator of $\Theta$ can achieve. The CRLB can thus be used to calculate the best CRT that can be obtained, given the pertinent properties of the crystal and photosensor. A complete discussion of the CRLB analysis in this context is given by Seifert et al. [28] and has been summarized by Schaart [1]. The parameters needed to compute the CRLB on the CRT are the number of detected photons, the scintillator rise time and decay time constants, and the single-photon time resolution (SPTR) of the photsensor. The light yields and decay times for the calculations were measured directly by the DPC and PMT setups respectively for each generation. The SPTR of two pixels in coincidence on the DPC has been measured by Brunner et al. [29] and Liu et al. [30], and found to be around 100 ps. This value was therefore taken as the SPTR for the calculation. Rise time data on the various generations was unavailable, and so was approximated to be 50 ps for all crystals. This choice was informed by previously reported values for similar crystals [11,15,31–37]. Based on the measured parameters, the calculated CRLB values for generations 2, 4, and 5 using first-photon triggering were 125 ps FWHM, 124 ps FWHM, and 119 ps FWHM, respectively. CRLB analysis thus predicted that generation 5 crystals would offer the best CRT performance, but did not anticipate the measured difference in CRT measurements between generations

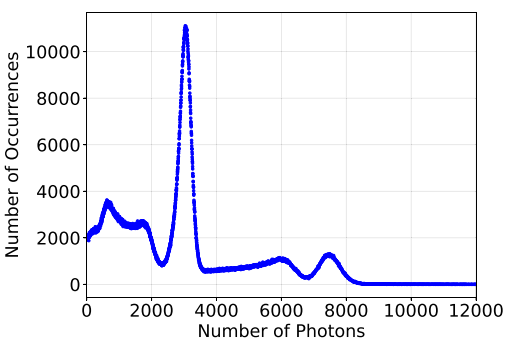


(a) Generation 2

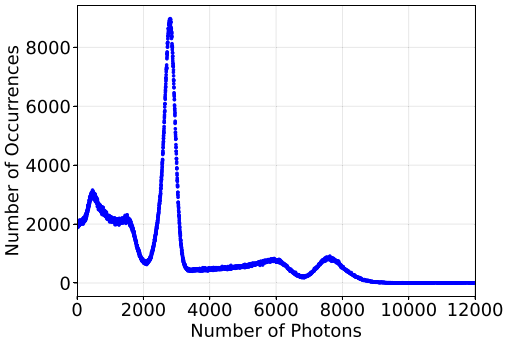


(b) Generation 4

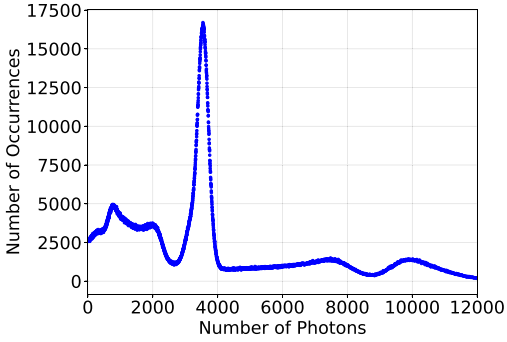


(c) Generation 5

**Fig. 11.** Examples of spectra recorded from the three different generations of crystals subjected to a 0.9 MBq $^{22}$Na source.

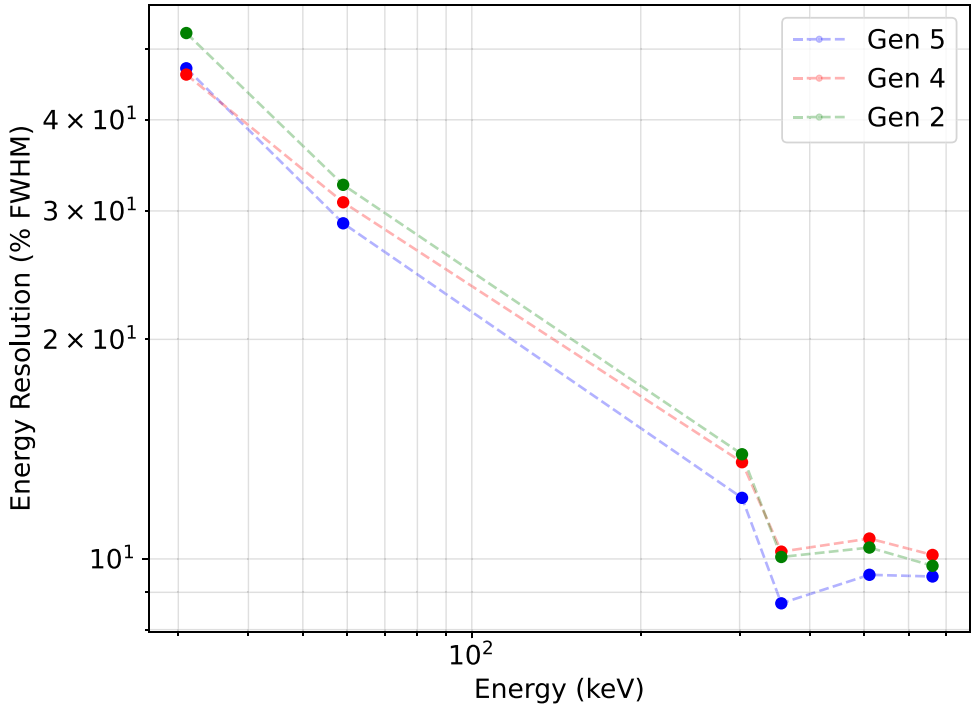


**Fig. 12.** Energy resolution measurements for the three generations of LYSO crystals at room temperature conducted on the DPC. Dashed lines are drawn between points to aid the eye.

2 and 4. Although accurate values for the $Ca^{2+}$ concentration of the crystals were not available, it is known that the generation 2 crystals had the lowest concentration, generation 5 crystals had the highest concentration, and generation 4 had an intermediate concentration relative to the other two. While rise time is not determined in this work, several studies have measured rise times in LSO and LYSO samples with and without $Ca^{2+}$ co-doping [38–41]. These measurements allow for the hypothesis that a sufficiently high $Ca^{2+}$ concentration improves

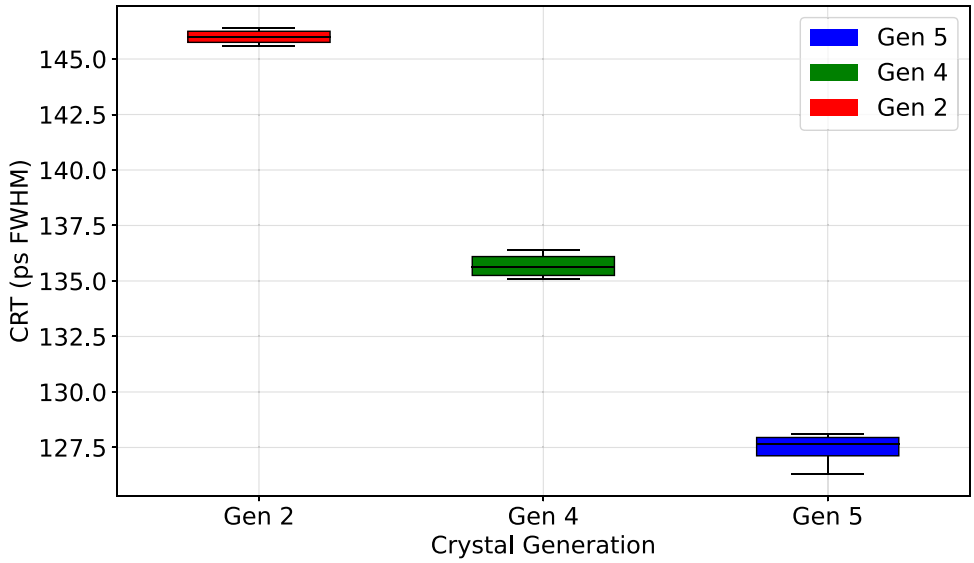


**Fig. 13.** CRT measurements for the three generations taken at −25 °C.

**Table 1**
LYSO light yield and decay time comparison. The values presented are the averages for each crystal. The errors are given as one standard deviation of the measured data, and thus represent the variation across the investigated crystals.

| Gen. | Light yield (photons/MeV) | Decay time (ns) |
|---|---|---|
| 2 | 21,700 ± 200 | 35.9 ± 0.8 |
| 4 | 22,900 ± 200 | 33.3 ± 0.3 |
| 5 | 22,500 ± 300 | 33.6 ± 0.9 |

**Table 2**
LYSO generation comparison when coupled with a Philips 3200-22-44 DPC. The values presented are the averages for each crystal or crystal pair. The errors on the experimental results are given as one standard deviation of the measured data, and thus represent the variation across the investigated crystals. The errors on the CRLB predictions are calculated by evaluating the CRT assuming a lower limit of 20 ps and an upper limit of 80 ps for the rise time (see text for further explanation).

| Gen. | Photopeak position (No. activated SPADs) | Energy resolution at 511 keV (% FWHM) | CRT (ps FWHM) | CRLB prediction (ps FWHM) |
|---|---|---|---|---|
| 2 | 2667 ± 30 | 10.4 ± 0.3 | 146.0 ± 0.3 | 125 ± 10 |
| 4 | 2519 ± 69 | 10.7 ± 0.1 | 135.7 ± 0.5 | 124 ± 10 |
| 5 | 2912 ± 18 | 9.5 ± 0.1 | 127.4 ± 0.7 | 119 ± 10 |
| LSO | 2605 ± 190 | 10.5 ± 0.7 | 129.7 ± 5.4 | 124 ± 10 |

the rise time by several tens of picoseconds, even though further investigations may be required to confirm this trend. For this reason, the generation 2 crystals may have a rise time more similar to a classical material without co-doping (between 50 ps and 100 ps), whereas the generations 4 and 5 crystals may have a shorter rise time (< 50 ps). The improved CRT performance of generation 4 over generation 2 could be explained by this [42]. An error of 10 ps was determined for the CRLB calculations by evaluating the CRT using a value of 20 ps as the lower limit on the rise time, and 80 ps as the upper limit. A difference in rise time on the order of tens of picoseconds due to $Ca^{2+}$ co-doping would therefore explain the CRT improvement between generation 2 and 4 crystals.

## 4. Conclusions

We characterized 3.3 mm × 3.3 mm × 3.3 mm and 3.3 mm × 3.3 mm × 5 mm LYSO crystals from Luxium Solutions' 2nd, 4th, and 5th generations in terms of light yield, decay time, non-proportionality, and emission spectrum. We then coupled the crystals with a Philips 3200-22-44 DPC and measured the number of SPADs triggered per scintillation event, the temperature dependence of the number of detected SPADs, the energy resolution at 511 keV and other energies, and the CRT. This was done with the aim of determining which of the materials would yield the best performance when incorporated into a dual-panel PET detector utilizing the Philips 3200-22-44 DPC (see Table 2).

The latter two generations are found to have markedly better characteristics, with similar improvements in light yield and decay time. When coupled to the DPC however, the generation 5 crystals significantly outperform the generation 4 crystals due to the better matching of the emission spectrum with the PDE of the detector. Additionally, this poorer performance may be further explained by the shorter wavelengths in the spectrum of the generation 4 crystals (Fig. 7), being more susceptible to absorption by any imperfections on the Teflon wrapping or crystal surfaces. Were the crystals intended for use with an SiPM with a different PDE curve, it is possible that the generation 4 crystals would be the optimal choice, given their slightly higher light yield.

It should be noted that the uncertainty in each set of measurements was found to be very low. The uncertainties were determined by calculating the standard deviation of each set of measured data, and so they do not account for potential systematic errors. Nevertheless, this demonstrates a high level of consistency and uniformity across crystals within the same generation.

## CRediT authorship contribution statement

**Jack Wehr:** Writing – review & editing, Writing – original draft, Visualization, Validation, Software, Methodology, Investigation, Formal analysis, Data curation, Conceptualization. **J. Jasper van Blaaderen:** Writing – review & editing, Methodology, Formal analysis. **Coen R.N. Rasch:** Writing – review & editing, Supervision, Project administration, Funding acquisition. **Dennis R. Schaart:** Writing – review & editing, Supervision, Resources, Project administration, Methodology, Investigation, Funding acquisition, Conceptualization.

## Declaration of competing interest

The authors declare the following financial interests/personal relationships which may be considered as potential competing interests: Jack Wehr reports financial support was provided by Dutch Cancer Society. If there are other authors, they declare that they have no known competing financial interests or personal relationships that could have appeared to influence the work reported in this paper.

## Acknowledgments

We thank Ralf Schulze and Thomas Frach from Philips Digital Photon Counting for technical support and advice in operating the Philips DPCs. We also thank Jan Huizenga from the MPT group for help with the thermal regulation of the detectors, and Kevin Kamman from DEMO in TU Delft for support in coupling the crystals to the DPC tiles. We would also like to thank Luxium Solutions, who kindly provided the crystals. This work was financially supported by the Dutch Cancer Society (KWF Kankerbestrijding), The Netherlands, grant No. 2020-1/13103.

## Data availability

Data will be made available upon request. Scripts used for the determination of the Cramer–Rao Lower Bound analysis are available online and are referenced in the manuscript.

## References

[1] Dennis R. Schaart, Physics and technology of time-of-flight PET detectors, Phys. Med. Biol. 66 (2021).
[2] P. Cambraia Lopes, J. Bauer, A. Salomon, I. Rinaldi, V. Tabacchini, T. Tessonnier, P. Crespo, K. Parodi, D.R. Schaart, First in situ TOF-PET study using digital photon counters for proton range verification, Phys. Med. Biol. 61 (16) (2016) 6203–6230.
[3] Katia Parodi, Vision 20/20: Positron emission tomography in radiation therapy planning, delivery, and monitoring, Med. Phys. (2015).
[4] Katia Parodi, In Vivo range verification in particle therapy, Med. Phys. (2018).
[5] Katia Parodi, Taiga Yamaya, Pawel Moskal, Experience and new prospects of PET imaging for ion beam therapy monitoring, Z. Med. Phys. 33 (1) (2023) 22–34, Special Issue: Recent Developments in Nuclear Medicine Imaging and Therapy.
[6] Aafke Christine Kraan, Range verification methods in particle therapy: Underlying physics and Monte Carlo modeling, Front. Oncol. 5 (2015) 150.
[7] Antje-Christin Knopf, Antony Lomax, In vivo proton range verification: a review, Phys. Med. Biol. 58 (15) (2013) R131–60.
[8] Xuping Zhu, Georges El Fakhri, Proton therapy verification with PET imaging, Theranostics 3 (10) (2013) 731–740.
[9] Paulo Crespo, Georgy Shakirin, Fine Fiedler, Wolfgang Enghardt, Andreas Wagner, Direct time-of-flight for quantitative, real-time in-beam PET: a concept and feasibility study, Phys. Med. Biol. 52 (23) (2007) 6795–6811.
[10] S. Surti, J.S. Karp, Design considerations for a limited angle, dedicated breast, TOF PET scanner, Phys. Med. Biol. 53 (11) (2008) 2911.
[11] Merry A. Spurrier, Piotr Szupryczynski, Kan Yang, A. Andrew Carey, Charles L. Melcher, Effects of $\hbox {Ca}^{2+}$ co-doping on the scintillation properties of LSO:Ce, IEEE Trans. Nucl. Sci. 55 (3) (2008) 1178–1182.
[12] Herman van Dam, Giacomo Borghi, Stefan Seifert, Dennis Schaart, Sub-200 ps CRT in monolithic scintillator PET detectors using digital SiPM arrays and maximum likelihood interaction time estimation, Phys. Med. Biol. 58 (2013) 3243–3257.
[13] Giacomo Borghi, Valerio Tabacchini, René Bakker, Dennis R. Schaart, Sub-3 mm, near-200 ps TOF/DOI-PET imaging with monolithic scintillator detectors in a 70 cm diameter tomographic setup, Phys. Med. Biol. 63 (15) (2018) 155006.
[14] Johan T.M. de Haas, Pieter Dorenbos, Advances in yield calibration of scintillators, IEEE Trans. Nucl. Sci. 55 (3) (2008) 1086–1092.
[15] David N. Ter Weele, Dennis R. Schaart, Pieter Dorenbos, Intrinsic scintillation pulse shape measurements by means of picosecond x-ray excitation for fast timing applications, Nucl. Instrum. Methods Phys. Res. Sect. A: Accel. Spectrom. Detect. Assoc. Equip. 767 (2014) 206–211.
[16] J. Jasper van Blaaderen, Daniel Biner, Karl W. Krämer, Pieter Dorenbos, The temperature dependent optical and scintillation characterisation of Bridgman grown $CsPbX_3$ (X=Br, Cl) single crystals, Nucl. Instrum. Methods Phys. Res. Sect. A: Accel. Spectrom. Detect. Assoc. Equip. 1064 (2024) 169322.
[17] Casper van Aarle, Karl W. Krämer, Pieter Dorenbos, Avoiding concentration quenching and self-absorption in $Cs_4EuX_6$ (X=Br, I) by $Sm^{2+}$ doping, J. Mater. Chem. C 11 (2023) 2336–2344, Open Access.
[18] Thomas Frach, Gordian Prescher, Carsten Degenhardt, Rik de Gruyter, Anja Schmitz, Rob Ballizany, The digital silicon photomultiplier — Principle of operation and intrinsic detector performance, in: 2009 IEEE Nuclear Science Symposium Conference Record, NSS/MIC, 2009, pp. 1959–1965.
[19] Carsten Degenhardt, Ben Zwaans, Thomas Frach, Rik Gruyter, Arrays of digital Silicon Photomultipliers — Intrinsic performance and application to scintillator readout, IEEE Nucl. Sci. Symp. Conf. Rec. Nucl. Sci. Symp. (2010).
[20] Dennis R. Schaart, Edoardo Charbon, Thomas Frach, Volkmar Schulz, Advances in digital SiPMs and their application in biomedical imaging, Nucl. Instrum. Methods Phys. Res. Sect. A: Accel. Spectrom. Detect. Assoc. Equip. 809 (2016) 31–52, Advances in detectors and applications for medicine.
[21] Herman T. van Dam, Stefan Seifert, Dennis R. Schaart, The statistical distribution of the number of counted scintillation photons in digital silicon photomultipliers: model and validation, Phys. Med. Biol. 57 (15) (2012) 4885.
[22] S. Kumar, D. Durini, C. Degenhardt, S. van Waasen, Photodetection characterization of SiPM technologies for their application in scintillator based neutron detectors, J. Instrum. 13 (01) (2018) C01042.
[23] W. Chewpraditkul, L. Swiderski, M. Moszynski, T. Szczesniak, A. Syntfeld-Kazuch, C. Wanarak, P. Limsuwan, Scintillation properties of LuAG:Ce, YAG:Ce and LYSO:Ce crystals for gamma-ray detection, IEEE Trans. Nucl. Sci. 56 (6) (2009) 3800–3805.
[24] C. Wanarak, W. Chewpraditkul, A. Phunpueok, Light yield non-proportionality and energy resolution of Lu1.95Y0.05SiO5:Ce and Lu2SiO5:Ce scintillation crystals, Procedia Eng. 32 (2012) 765–771, ISEEC.
[25] Ivan V. Khodyuk, Pieter Dorenbos, Trends and patterns of scintillator nonproportionality, IEEE Trans. Nucl. Sci. 59 (6) (2012) 3320–3331.
[26] W.W. Moses, S.A. Payne, W.-S. Choong, G. Hull, B.W. Reutter, Scintillator non-proportionality: Present understanding and future challenges, IEEE Trans. Nucl. Sci. 55 (3) (2008) 1049–1053.
[27] Jack Wehr, Cramer-rao lower bound for coincidence resolving time of scintillator detectors, 2025, https://doi.org/10.6084/m9.figshare.28945925. (Accessed 07 May 2025).
[28] Stefan Seifert, Herman Dam, Dennis Schaart, The lower bound on the timing resolution of scintillation detectors, Phys. Med. Biol. 57 (2012) 1797–1814.
[29] S. Brunner, Lukas Gruber, Albert Hirtl, K. Suzuki, Johann Marton, Dennis Schaart, A comprehensive characterization of the time resolution of the Philips Digital Photon Counter, J. Instrum. 11 (2016) P11004.
[30] Zile Liu, Stefan Gundacker, Marco Pizzichemi, A. Ghezzi, Etiennette Auffray, Marco Paganoni, In-depth study of single photon time resolution for the Philips digital silicon photomultiplier, J. Instrum. 11 (2016) P06006.
[31] Stefan Gundacker, Etiennette Auffray, Kristof Pauwels, Paul Lecoq, Measurement of intrinsic rise times for various L(Y)SO and LuAG scintillators with a general study of prompt photons to achieve 10 ps in TOF-PET, Phys. Med. Biol. 61 (7) (2016) 2802–2837.
[32] S. Gundacker, F. Acerbi, E. Auffray, A. Ferri, A. Gola, M.V. Nemallapudi, G. Paternoster, C. Piemonte, P. Lecoq, State of the art timing in TOF-PET detectors with LuAG, GAGG and L(Y)SO scintillators of various sizes coupled to FBK-SiPMs, J. Instrum. 11 (08) (2016) P08008.
[33] S. Gundacker, R.M. Turtos, E. Auffray, P. Lecoq, Precise rise and decay time measurements of inorganic scintillators by means of X-ray and 511 keV excitation, Nucl. Instrum. Methods Phys. Res. Sect. A: Accel. Spectrom. Detect. Assoc. Equip. 891 (2018) 42–52.
[34] Kan Yang, Charles L. Melcher, Philip D. Rack, Lars A. Eriksson, Effects of calcium codoping on charge traps in LSO:Ce crystals, IEEE Trans. Nucl. Sci. 56 (5) (2009) 2960–2965.
[35] S.E. Derenzo, J. Weber, W.W. Moses, C. DuJardin, Measurements of the Intrinsic Rise Times of Common Inorganic Scintillators.
[36] L. Pidol, A. Kahn-Harari, B. Viana, E. Virey, B. Ferrand, P. Dorenbos, J.T.M. De Haas, C.W.E. Van Eijk, High efficiency of lutetium silicate scintillators, Ce-doped LPS, and LYSO crystals, IEEE Trans. Nucl. Sci. 51 (3) (2004) 1084–1087.
[37] S. Seifert, J.H.L. Steenbergen, H.T. Van Dam, D.R. Schaart, Accurate measurement of the rise and decay times of fast scintillators with solid state photon counters, J. Instrum. 7 (09) (2012) P09004.

[38] Stefan Gundacker, Etiennette Auffray, Kristof Pauwels, Paul Lecoq, Measurement of intrinsic rise times for various L(Y)SO and LuAG scintillators with a general study of prompt photons to achieve 10 ps in TOF-PET, Phys. Med. Biol. 61 (7) (2016) 2802.

[39] Stefan Gundacker, Rosana Martinez Turtos, Nicolaus Kratochwil, Rosalinde Pots, Marco Paganoni, Etiennette Auffray, Experimental time resolution limits of modern SiPMs and TOF-PET detectors exploring different scintillators and Cherenkov emission, Phys. Med. Biol. (2020).

[40] S. Gundacker, R.M. Turtos, E. Auffray, P. Lecoq, Precise rise and decay time measurements of inorganic scintillators by means of X-ray and 511 keV excitation, Nucl. Instrum. Methods Phys. Res. Sect. A: Accel. Spectrom. Detect. Assoc. Equip. 891 (2018) 42–52.

[41] David N. Ter Weele, Dennis R. Schaart, Pieter Dorenbos, Scintillation properties of Ca co-doped L(Y)SO:Ce between 193 K and 373 K for TOF-PET/MRI, EJNMMI Phys. 1 (Suppl 1) (2014) A10.

[42] Merry A. Spurrier, Piotr Szupryczynski, Kan Yang, A. Andrew Carey, Charles L. Melcher, Effects of $Ca^{2+}$ co-doping on the scintillation properties of LSO:Ce, IEEE Trans. Nucl. Sci. 55 (3) (2008) 1178–1182.